

# On-the-fly green generation and dispersion of AgI nanoparticles for cloud seeding nuclei

Xiuli Hu · Wenbo Zhou · Xizheng Wang ·  
Tao Wu · Jeffery B. Delisio · Michael R. Zachariah

Received: 10 December 2015 / Accepted: 22 July 2016 / Published online: 29 July 2016  
© Springer Science+Business Media Dordrecht 2016

**Abstract** This study reports on an on-the-fly green synthesis/dispersion of silver iodide (AgI) nanoparticles from the combustion of AgIO<sub>3</sub>/carbon black (CB)/nitrocellulose (NC) composites, which could be used as a candidate for a cloud-seeding pyrotechnic. Films were formed by direct electrospray deposition of a mixture of synthesized silver iodate with CB and NC. The decomposition pathways of AgIO<sub>3</sub>/CB and AgIO<sub>3</sub>/CB/NC were evaluated by temperature jump time of flight mass spectrometry (T-jump TOFMS) and XRD, showing that AgI particles and CO<sub>2</sub> are released from the reaction between AgIO<sub>3</sub> and CB without other toxic residuals. The flame propagation velocity of AgIO<sub>3</sub>/CB/NC films increases with the increasing of particle mass loading of AgIO<sub>3</sub> and CB and peaks at 40 wt%, which is much higher than that of an AgI/AP/NC film. The mean diameter of the resultant AgI nanoparticles is from 51 to 97 nm. The

mass loading of AgIO<sub>3</sub> and CB was found to play a major role in size control of the AgI nanoparticles.

**Keywords** Silver iodate · Cloud seeding pyrotechnic · Silver iodide · Electrospray deposition · Aerosol · Weather

## Introduction

Over the past century, various attempts have been made to modify local weather patterns to moderate extreme weather events (e.g., hail) and change local drought conditions (Ryan and King 1997; Changnon 1977; Federer and Schneider 1981). Following the classic experiments of Schaefer (1946) in the United States (Guo et al. 2006; Orville 1996; Orville et al. 1984), various weather modification activities have been explored for precipitation enhancement. Homogeneous and heterogeneous nucleation processes are the two main mechanisms for ice nucleation. The former generates ice crystals by rapid cooling, while the latter generates ice-forming nuclei. For example, dry ice (Ryan and King 1997; Dennis 1980), liquid carbon dioxide (Guo et al. 2006), and liquid nitrogen are coolants, while composite pyrotechnics with silver iodide (AgI) can be used as an ice-forming nuclei (Blair et al. 1973; DeMott 1988; Sax et al. 1979; Sullivan et al. 2011). AgI has been found to be the most effective condensation nuclei, because the lattice

**Electronic supplementary material** The online version of this article (doi:10.1007/s11051-016-3528-5) contains supplementary material, which is available to authorized users.

X. Hu · W. Zhou · X. Wang · T. Wu ·  
J. B. Delisio · M. R. Zachariah (✉)  
Department of Chemical and Biomolecular Engineering,  
University of Maryland, College Park, MD 20742, USA  
e-mail: mrz@umd.edu

X. Hu · W. Zhou · X. Wang · T. Wu ·  
J. B. Delisio · M. R. Zachariah  
Department of Chemistry and Biochemistry, University of  
Maryland, College Park, MD 20742, USA

parameters of its hexagonal crystal habit conform closely to that of ice (Dennis 1980; Vonnegut 1947; Weather Modification Association WMA 2009; Burley 1963). Many methods have been used to generate AgI aerosol, including combustion of AgI/NH<sub>4</sub>I, AgI/KI, AgI/NaI acetone solutions (Blair et al. 1973), combustion of pyrotechnics of AgI/NH<sub>4</sub>ClO<sub>4</sub>/NC, NH<sub>4</sub>ClO<sub>4</sub>/KI/AgI/phenolic resin, Al/KMnO<sub>4</sub>/AgI/NC, NH<sub>4</sub>ClO<sub>4</sub>/PbI<sub>2</sub>/AgI/Organic binder, AgIO<sub>3</sub>/KIO<sub>3</sub>/Mg/Al/Sr(NO<sub>3</sub>)<sub>2</sub>/polyester binder, and AgIO<sub>3</sub>/Mg/Al/epoxy binder (Federer and Schneider 1981; Sax et al. 1979; Su 2008; Liu et al. 2011; Mather et al. 1997).

Unfortunately, there are still some shortcomings in the application of these materials to generate AgI aerosol in situ. For example, since the combustion velocity of AgI/KI acetone solution is slow, the production rate of AgI aerosol is low (Su 2008). Alternatively the logistics of handling hygroscopic NH<sub>4</sub>ClO<sub>4</sub> and NaClO<sub>4</sub> have made the formulation with hygroscopic salt less attractive than other materials (Biswas and Dennis 1971). The hygroscopic particles tend to agglomerate in the pyrotechnic which also can reduce the efficiency of the nucleation. Long-term storage issues also arise for Al- and Mg-based thermite pyrotechnic, since the hygroscopic nature of NH<sub>4</sub>ClO<sub>4</sub> is acidic. In our previous research (Sullivan et al. 2012; Egan et al. 2014; Jian et al. 2013), fuel nanoparticle aggregates upon heating experience preignition sintering, giving micron-sized particles which can reduce the efficiency of the nucleation. Ideally, one would like a material which has a combustion flame temperature higher than 1770 K for the sublimation of AgI, undergoes stable combustion, is simple to fabricate, and releases AgI aerosol with minimal toxic by-products.

If we consider the combustion of AgIO<sub>3</sub> and CB, equilibrium calculations show an adiabatic flame temperature of ~3500.0 K (Westrum and Arbor 1989; Turns 2000) (The calculation is detailed in the Supplement 1 (Table S1)), with only AgI and CO<sub>2</sub> as products. Operationally, solid energetic composites require a suitable binder system, which for our evaluation purposes is a thin film using NC as the binder. NC is chosen as the binder because of the high nontoxic gas production rate, which could serve as an aerosol dispersant. A direct deposition method (Electrospray or electrohydrodynamic deposition) was applied to obtain composite films containing AgIO<sub>3</sub>, CB, and NC, which enables the eventual ability to make graded and laminate structures at high particle

loadings (Li et al. 2015). AgIO<sub>3</sub>/Al/NC and AgI/AP/NC films were also analyzed and compared to the more desirable AgIO<sub>3</sub>/CB/NC film. In principle, the AgIO<sub>3</sub>/CB/NC can be considered as a simultaneous route to create the AgI nucleation seed source with a vigorous gaseous emitter to aid in dispersion. The solid composite has good handling properties making it amenable to be employed in droppable pyrotechnics, rockets, and ground-based airborne generation.

## Experimental

### Materials

Carbon black (CB) used in this work was purchased from Cabot Corporation (CAS registry number: 1333-86-4). Silver nitrate solution N/10 (AgNO<sub>3</sub>) with a concentration of 16.99 mg AgNO<sub>3</sub>/mL was purchased from Fisher Scientific. N–N-Dimethylformamide (DMF) (99.8 wt%), ammonium perchlorate (AP) (99.8 wt%), potassium iodate (KIO<sub>3</sub>) (99.5 wt%), and silver iodide (AgI) (99.0 wt%) were directly used as-received from Sigma-Aldrich. Collodion solution was purchased from Fluka with a concentration of 4–8 wt% in 3:1 ethanol/diethyl ether, and 50 mL was carefully dried in fume hood for further use as solid nitrocellulose. The aluminum nanoparticles (Al-NPs) (Alex, 85 nm) were purchased from NovaCentrix with an active Al content of 81 % by mass, and were determined by thermogravimetric analysis (TGA).

### Synthesis of AgIO<sub>3</sub>

Silver iodate was synthesized by a wet chemistry method. 75 mL 0.0001 M silver nitrate solution and 75 mL 0.000101 M potassium iodate solution were mixed dropwise (5 mL/min) under vigorous stirring. As the KIO<sub>3</sub> solution was added, a white precipitate immediately formed which was subsequently collected by centrifugation. The product was washed three times with DI water and ethanol, respectively, dried in a fume hood for 12 h, and then grounded into a fine powder by using a mortar and pestle (Pearce and Wirth 1933) (Sullivan et al. 2011).

### Precursor preparation

The synthesized AgIO<sub>3</sub> particles were dispersed in DMF with 30 min ultrasonication, and then CB

particles were gently added, followed by another 30 min ultrasonication. In a typical process, 58.8 mg of AgIO<sub>3</sub> particles, 3.8 mg CB powder, and 250 mg prepared NC were dissolved in 5 mL DMF. The suspension obtained above was sonicated for another 30 min, followed by 24 h magnetic stirring before use. The films of AgIO<sub>3</sub>/Al/NC, AgI/AP/NC were prepared as references, and the formulations of all the films used in this study are displayed in Table S2 in Supplement 1.

### Film deposition

Films were deposited using electrospray method, which was previously used by our group (Li et al. 2015; Huang et al. 2015), and the schematic illustration of the film deposition system is displayed in the Supplement 1 (Fig. S1). In this work, a feeding rate of 2 mL/h was chosen to feed the precursor with a syringe pump through a flat-tip stainless needle with a 0.43-mm inner diameter, under an 18-kV working voltage. A 4.5-cm jet-to-substrate distance was employed to allow for some solvent evaporation prior to deposition. The conductive aluminum foil on a rotating drum was used as the substrate for films, which enabled easy generation of free-standing films. SAFETY NOTE: The electrospray apparatus was shielded in an insulated box to avoid the possible dangers of high voltage and spark ignition with a interlock switch.

### Characterization

X-ray diffraction (XRD) was used to obtain the crystal structure of AgIO<sub>3</sub> and postcombustion products with a Bruker C2 Discover with General Area Detector Diffraction System, operating at 40 kV and 40 mA with unfiltered Cu K $\alpha$  radiation, E $\lambda$ 4049 eV, k $\lambda$ 1.5406 Å.

Scanning electron microscopy (SEM) was conducted with a Hitachi, Su70 FEG-SEM to acquire the morphology of AgIO<sub>3</sub>, structures of films, and particle size of postcombustion product. For cross section imaging, the film was fractured in liquid nitrogen and then cleaved.

Temperature jump time of flight mass spectrometry (T-jump TOFMS) was performed using the previously described home-built instrument (Jian et al. 2013; Zhou et al. 2009, 2010) to obtain speciation during rapid heating and ignition temperature. For these

samples, they were electrospray deposited onto a 76- $\mu$ m diameter platinum wire which was heated at  $\sim 6 \times 10^5$  K s<sup>-1</sup> in about 3 ms. A sampling rate of 100  $\mu$ s per spectrum (10 kHz) captured the progress of the reaction with 95 spectra obtained posttriggering for each run. The data were sampled using a Teledyne-LeCroy 606Zi 600 MHz digital oscilloscope and transferred to a PC for further analysis.

The combustion events in air of the AgIO<sub>3</sub>/CB/NC, AgIO<sub>3</sub>/Al/NC, and AgI/AP/NC films were captured by a high-speed camera (Phantom Micro 110 Cameras, Vision Research Inc.) with a frame rate of 7000 frames per second. In a typical test, a 3  $\times$  0.5  $\times$  0.0065-cm specimen was fixed between a nichrome wire and a holder shown in our previous study (Li et al. 2015) and the Supplement 1 (Fig. S2) (three specimens were tested for each film) and ignited by resistively heating the nichrome wire triggered by an external DC power supply. PCC 1.2 software (Phantom, Inc.) was used to analyze the images from the camera and calculate the flame propagation velocity of the films.

The combustion residual of AgIO<sub>3</sub>/CB/NC film was collected by using a home-made setup displayed in Fig.S3 (Supplement 1). It was composed of three glass slides with one side sealed by aluminum foil. Two pieces of conductive tape were attached at the two upper slides with the same distance to the film to make sure there was no difference between different films. The film was ignited using a lighter and after the ignition, the combustion residuals were sputtered onto the conductive tape and analyzed by SEM.

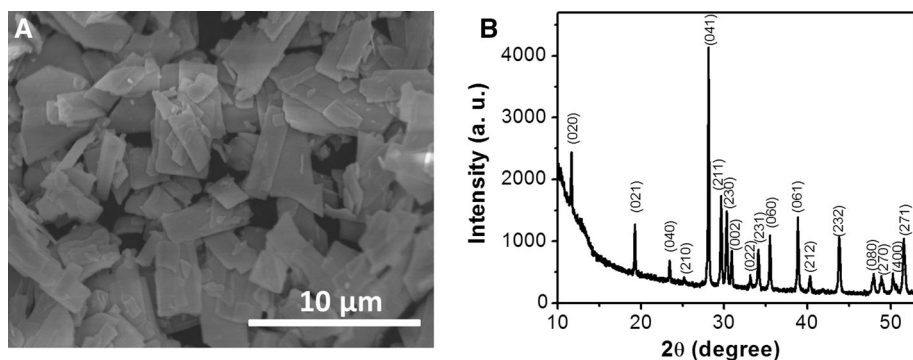
## Results and discussion

### Properties of AgIO<sub>3</sub>

The morphology and structure of the as-prepared AgIO<sub>3</sub> are presented in Fig. 1. The prepared AgIO<sub>3</sub> is flake-like with a wide particle size distribution from  $\sim 100$  nm to  $\sim 10$   $\mu$ m. XRD analysis was used to confirm that we were producing phase-pure AgIO<sub>3</sub> structure (ICDD PDF No. 45-0880).

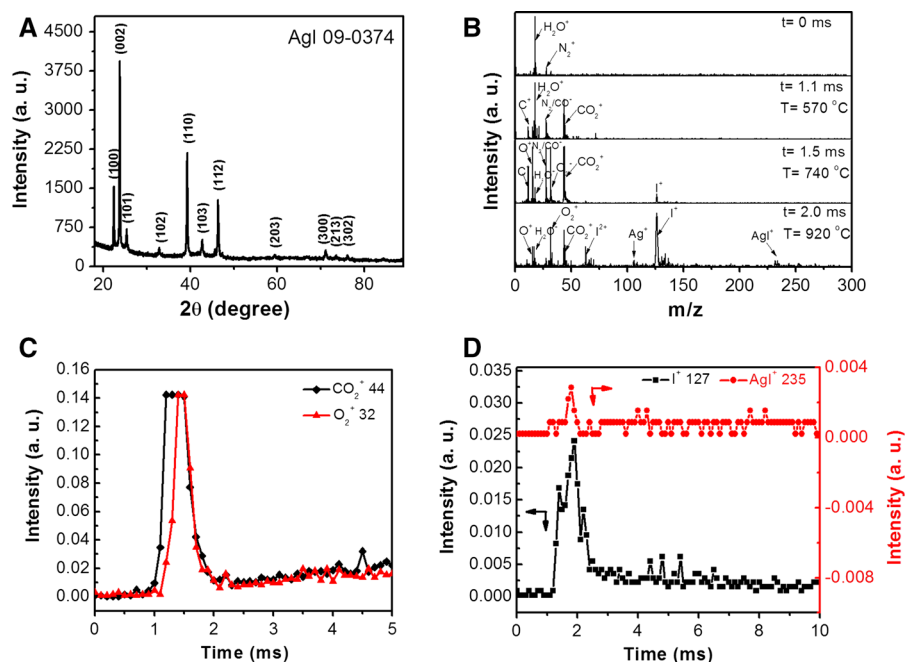
### Combustion and product analysis of AgIO<sub>3</sub>/CB composite

Figure 2a shows the XRD analysis of the reaction product and shows the product to, at least in the



**Fig. 1** SEM image (a) and XRD pattern (b) of prepared AgIO<sub>3</sub>

**Fig. 2** a XRD of post combustion product; b time-resolved mass spectra from reaction between AgIO<sub>3</sub> and CB at a heating rate of  $\sim 6 \times 10^5 \text{ K s}^{-1}$ ; c Temporal profile of CO<sub>2</sub><sup>+</sup>, O<sub>2</sub><sup>+</sup> and d I<sup>+</sup>, AgI<sup>+</sup> released upon rapid heating of AgIO<sub>3</sub>/CB composite



crystalline phase, be pure AgI (ICDD PDF No. 09-0374). The lattice constant of obtained AgI (ICDD PDF No. 09-0374) is  $4.5922 \times 7.51$ , which is close to that of ice ( $4.535 \times 7.41$ ) (Vonnegut 1947).

To probe the reaction mechanism between AgIO<sub>3</sub> and CB, time-resolved mass spectra were obtained during the rapid heating of pure AgIO<sub>3</sub> (Fig. S4) particles and AgIO<sub>3</sub>/CB composite (Fig. 2b). For this experiment, the heating duration was about 3 ms with heating rate of  $\sim 6 \times 10^5 \text{ K s}^{-1}$ . The decomposition temperature of pure AgIO<sub>3</sub> particle is 798 °C as shown in Fig S4. The obtained mass spectra of AgIO<sub>3</sub>/CB composite at 1.1 (570 °C), 1.5 (740 °C), 2.0 (920 °C)

ms are presented in Fig. 2b, along with the background spectrum taken at  $t = 0$  ms. The mass spectra taken at  $t = 1.1$  ms clearly shows carbon dioxide ( $m/z = 44$ ) produced upon rapid heating, which corresponds to the reaction between AgIO<sub>3</sub> and CB, showing that AgIO<sub>3</sub> reacts with CB in the condensed phase before the release of O<sub>2</sub> from AgIO<sub>3</sub> as shown in Fig. 3. At 1.5 ms (740 °C), the O<sup>+</sup>/O<sub>2</sub><sup>+</sup> ( $m/z = 16/32$ ) and I<sup>+</sup> ( $m/z = 127$ ) originate from the decomposition of AgIO<sub>3</sub>. These curves show that the onset temperature of O<sub>2</sub> release is  $\sim 740 \text{ K}$  at a heating rate of  $\sim 6 \times 10^5 \text{ K s}^{-1}$ . I<sup>2+</sup>, I<sup>+</sup>, Ag<sup>+</sup>, and AgI<sup>+</sup> appear simultaneously at 2.0 ms, which corresponds to the

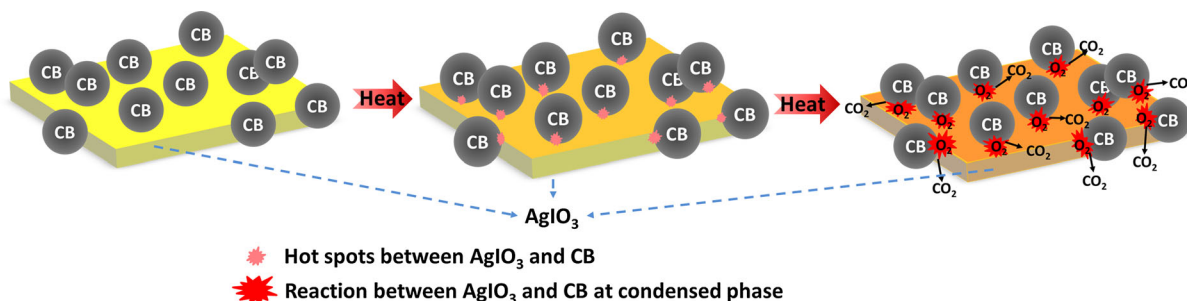


**Fig. 3** Proposed = reaction mechanism between  $\text{AgIO}_3$  and CB

decomposition and volatilization of AgI. No gas phase C containing species other than  $\text{CO}_2$  was identified. As presented in Fig. 2c,  $\text{CO}_2$  production is observed before  $\text{O}_2$ , implying direct reaction between  $\text{AgIO}_3$  and CB in the condensed phase compared with the temporal profile of  $\text{CO}_2^+$ ,  $\text{O}_2^+$  decomposed from pure  $\text{AgIO}_3$  as shown in Fig. S4 of Supplement 1, which demonstrates that the  $\text{CO}_2^+$  is not from the reaction between hexane and  $\text{O}_2$ . The possible reaction mechanism between  $\text{AgIO}_3$  and CB can be seen in Fig. 3. CB has a very high melting temperature ( $>3800$  K), and obviously not possessing an oxide shell is directly accessible to the  $\text{AgIO}_3$ . Thus a condensed phase reaction between  $\text{AgIO}_3$  and CB results in a much lower reaction temperature (570 C) than the decomposition temperature (798 C) of pure  $\text{AgIO}_3$  particles. We also note that no  $\text{I}_2$  is observed in the Supplement 1 Fig. S5, thus  $\text{I}^+$  seen is presumably from electron impact fragmentation of AgI in the mass spectrometer (Fig. 2d), and the curve of  $\text{AgI}^+$  follows that of  $\text{I}^+$  and they have the same trend.

#### Properties of $\text{AgIO}_3/\text{CB}/\text{NC}$ films

For cloud seeding pyrotechnic applications, a seeding aircraft or ground-based generator would be employed to generate AgI aerosol from a binder system rather than directly from powder. Here, we employ a film-architecture from direct deposition via electrospray. Direct deposition methods offer the potential to make graded material as well as material with high solids loadings in any shape (Zenin 1995; Wei et al. 2007; Meeks et al. 2014). We used an electrospray deposition method based on our prior work (Huang et al. 2015; Li et al. 2015). From the SEM images of the deposited  $\text{AgIO}_3/\text{CB}/\text{NC}$  film (Fig. 4 a, b), we can see that most

of the flake-like  $\text{AgIO}_3$  particles are horizontally layered within the film. We believe the alignment of these particles results from the wet deposition onto the rotating drum allowing for rearrangement. The post-combustion products of  $\text{AgIO}_3/\text{CB}/\text{NC}$  film with 20 wt% particle mass loading were collected, and their morphology is shown in Fig. 4c, d.

With particle mass loading of 20 wt%, the mean particle size of the post combustion product from  $\text{AgIO}_3/\text{CB}/\text{NC}$  film is  $\sim 62$  nm, while that of  $\text{AgI}/\text{AP}/\text{NC}$  and  $\text{AgIO}_3/\text{Al}/\text{NC}$  films are 72 and 455 nm, respectively shown in Table S4 in Supplement 1. The average sizes and size distributions of the AgI particles were determined based on the SEM images of the AgI aerosol using Nano Measurer 1.2 software (He et al. 2013; Yao et al. 2014). The diameter distributions of the postcombustion product of  $\text{AgIO}_3/\text{CB}/\text{NC}$  and  $\text{AgI}/\text{AP}/\text{NC}$  films are much smaller than that released from  $\text{AgIO}_3/\text{Al}/\text{NC}$  film (Fig. S6 and Table S4 in Supplement 1). As seen in Fig. S6 and Table S4 in Supplement 1, the combustion of  $\text{AgIO}_3/\text{Al}/\text{NC}$  films generated spherical particles with a wide size distribution from 80 nm to 2.5  $\mu\text{m}$  containing  $\text{Al}_2\text{O}_3$ . The agglomeration and condensation of the  $\text{Al}_2\text{O}_3$ , and the wide size distribution of the residual would affect the size distribution and condensation of AgI aerosol, which would impair the nucleation efficiency of the pyrotechnics.

Diameter and size distribution of an AgI aerosol both play important roles in the cloud seeding process. Therefore, the sizes and distribution of AgI released from the combustion of  $\text{AgIO}_3/\text{CB}/\text{NC}$  films with different mass loadings of  $\text{AgIO}_3$  and CB were obtained in Fig. 5. AgI aerosol size spectra analysis was calculated from image processing of the images obtained through electron microscopy. As shown in

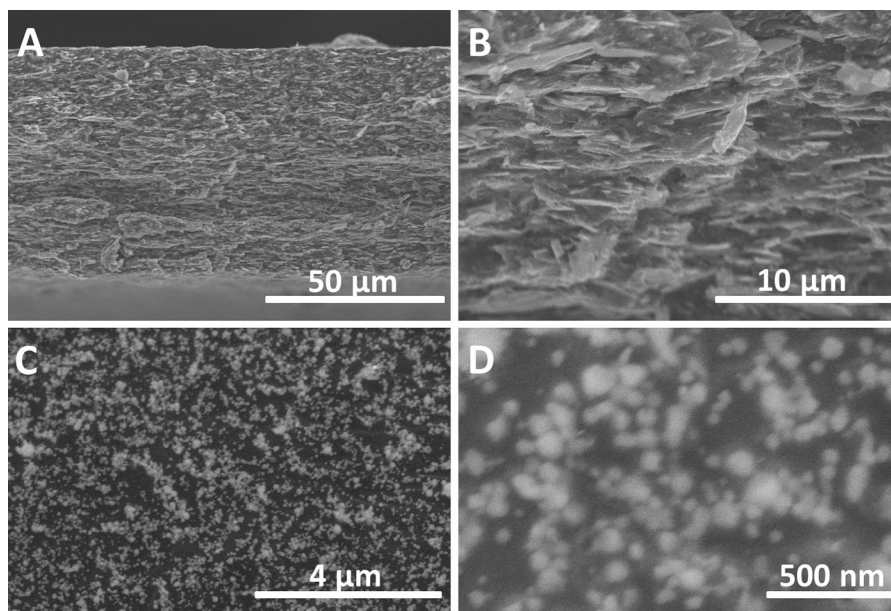


**Fig. 4** SEM images of film with 20 wt% mass loading and the postcombustion product, **a** cross section of AgIO<sub>3</sub>/CB/NC film; **b** close-up of film cross section; **c** Low magnification of the postcombustion product of AgIO<sub>3</sub>/CB/NC film; **d** High

magnification of the postcombustion product of AgIO<sub>3</sub>/CB/NC film (AgI particles decomposed when exposed under the beam, therefore the images are blurry)

Fig. 5, the mean diameter gradually increased to a larger size from 51 to 97 nm by increasing the mass loading of AgIO<sub>3</sub> and CB in the AgIO<sub>3</sub>/CB/NC films. Figure 5f shows the mean diameter and the counts of AgI particles per mol of AgIO<sub>3</sub> as a function of the mass loading of AgIO<sub>3</sub> and CB particles. This was calculated from the mean diameter and the number of AgI particles per mol of AgIO<sub>3</sub> (theoretically produced) as a function of the ratio of AgIO<sub>3</sub> and CB to NC. The number counts are determined from the average size and density, and varies from  $1 \times 10^{16}$  to  $7 \times 10^{16}$  particles per mol of AgIO<sub>3</sub>, with the largest value at the lowest AgI content used in the pyrotechnic. The size distribution of ice nucleus aerosols can be from 0.01 to 10 μm (Dennis 1980), and the smaller the particle formed, the higher the nucleation efficiency obtained. Therefore, AgIO<sub>3</sub>/CB/NC can be used as a candidate for cloud seeding pyrotechnic.

#### Combustion properties

For a cloud-seeding pyrotechnic, besides the particle size and distribution of AgI aerosol, combustion speed is another factor that should be considered. The flame propagation velocity was evaluated with a high-speed

camera for  $3 \times 0.5 \times 0.0065$  cm films and is shown in Fig. 6 as a function of the mass loading of AgIO<sub>3</sub>/CB particles. For AgIO<sub>3</sub>/CB/NC film, the flame propagation velocity in air increases with the increasing particle mass loading of AgIO<sub>3</sub> and CB, and peaks at about 40 wt% (AgIO<sub>3</sub>/CB over NC). At 60 wt%, no self-propagation in the film of AgIO<sub>3</sub>/CB/NC is evident. There is no self-propagation in the film of AgI/AP/NC shown in Table S4 (Supplement 1) with 20 wt% particle mass loading, while the propagation rate of AgIO<sub>3</sub>/Al/NC film with 20 wt% particle mass loading is 2.82 cm/s (Table S4 in supplement 1). Therefore, the film of AgIO<sub>3</sub>/Al/NC has almost the same propagation rate as that of AgIO<sub>3</sub>/CB/NC, but with very large mean diameter postcombustion product. Unfortunately, the combustion properties of AgI/AP/NC are too poor to warrant further consideration. In summary, the AgIO<sub>3</sub>/CB/NC film seems to show the best combination of particle generation and propagation speed.

#### Mechanism of combustion propagation

Video imaging of combustion of AgIO<sub>3</sub>/CB/NC film is quite different from that observed in our previous

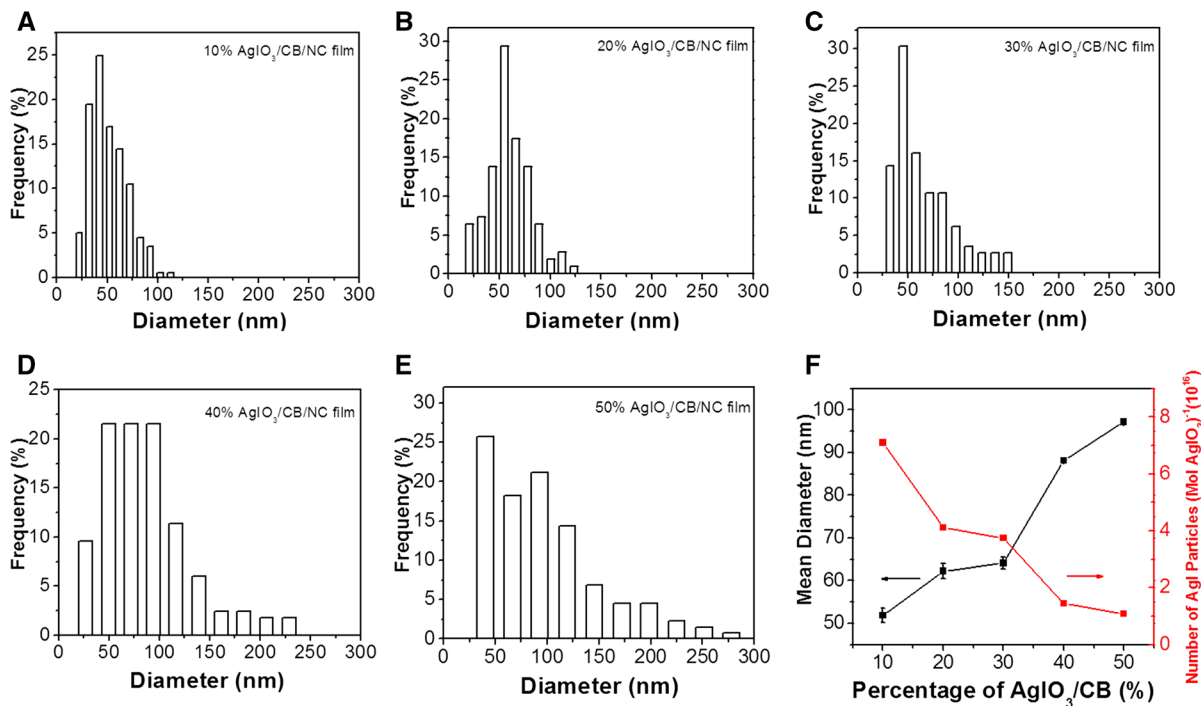


**Fig. 5** Statistical analyses of the sizes of the AgI nanoparticles with different percentages of AgIO<sub>3</sub> and CB: diameter distribution of 10 wt% (a), 20 wt% (b), 30 wt% (c), 40 wt%

(d), 50 wt% (e), the mean diameter of AgI particles and the number of AgI particles per mol of AgIO<sub>3</sub> with different mass loadings (f)

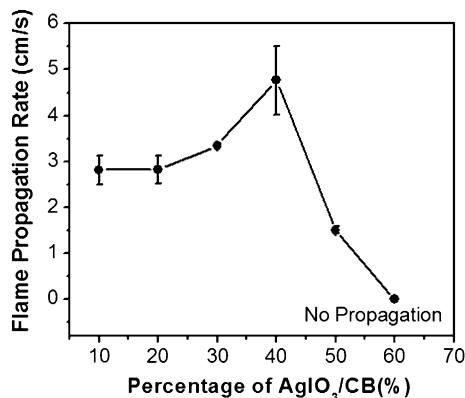


**Fig. 6** Propagation rates in air of AgIO<sub>3</sub>/CB/NC films

works (Al/PVDF, Bi(IO<sub>3</sub>)<sub>3</sub>/Al/PVDF, and CuO/Al/PVDF (Hu et al. 2016; Huang et al. 2015)) (In particular, we observe a two-zone flame in Supplement 2) as illustrated in Fig. 7. To probe the mechanism of the combustion propagation of AgIO<sub>3</sub>/CB/NC composite, T-jump TOFMS was conducted to investigate the time-resolved mass spectra of the pure NC, AgIO<sub>3</sub>/CB composite, and AgIO<sub>3</sub>/CB/NC

composite, respectively. From the analysis of the time-resolved mass spectra of pure NC, AgIO<sub>3</sub>/CB, and AgIO<sub>3</sub>/CB/NC film in Table 1, NO<sup>+</sup> is detected at 0.8 ms (430 K) which corresponds to the decomposition of NC. For AgIO<sub>3</sub>/CB, a sharp CO<sub>2</sub> peak is detected at 1.1 ms (570 K), presumably by direct reaction between AgIO<sub>3</sub> and CB, while at 1.5 ms (740 K) the decompositions of AgIO<sub>3</sub>, Ag<sup>+</sup>, I<sup>+</sup>, O<sup>+</sup>, O<sub>2</sub><sup>+</sup> are observed. This is consistent with the results seen for the complete AgIO<sub>3</sub>/CB/NC system. For AgIO<sub>3</sub>/CB/NC system, NO<sup>+</sup> is obtained at 0.8 ms (360 K) showing that the decomposition temperature of NC is lower than that of pure NC, which corresponds to the catalysis of AgIO<sub>3</sub> and CB. At 1.5 ms (670 K), a significant peak of CO<sub>2</sub><sup>+</sup> was detected due to the reaction between AgIO<sub>3</sub> and CB. The final decomposition of AgIO<sub>3</sub> occurs at 1.6 ms (710 K) and the peaks of Ag<sup>+</sup>, I<sup>+</sup>, O<sup>+</sup>, O<sub>2</sub><sup>+</sup> are observed, respectively. This implies that the first flame front is consistent with the decomposition of NC and its reaction with O<sub>2</sub>. The secondary flame front is consistent with the reaction of AgIO<sub>3</sub> and CB, and the decomposition of AgIO<sub>3</sub> with AgI nanoparticle

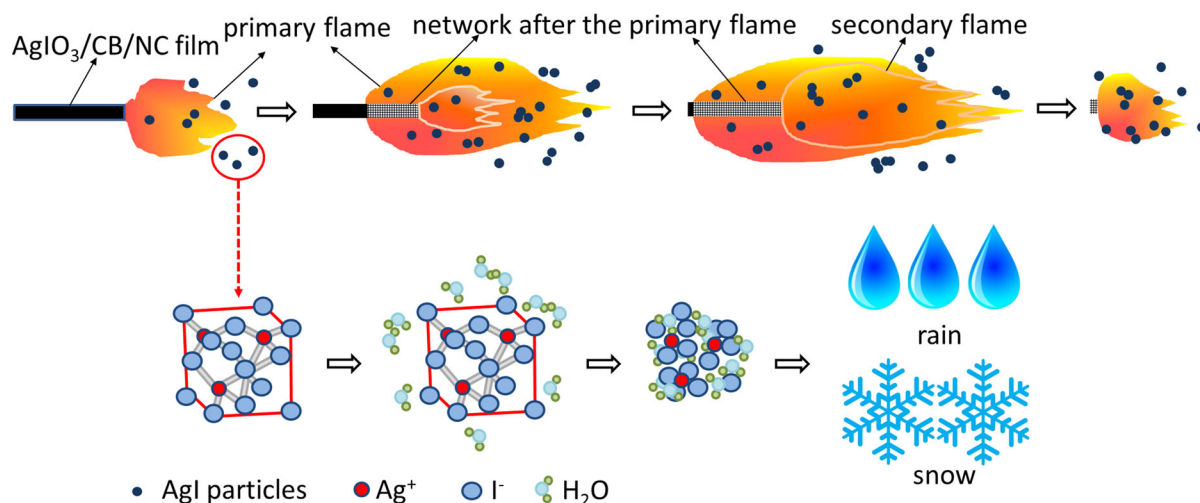


**Fig. 7** Schematic structure of the propagation flame of  $\text{AgIO}_3/\text{CB}/\text{NC}$  film and the possible formation process of rain or snow

**Table 1** Decomposition/reaction time, decomposition/reaction temperature, and the species released from NC,  $\text{AgIO}_3/\text{CB}$ , and  $\text{AgIO}_3/\text{CB}/\text{NC}$

Sample	Decomposition/ reaction time (ms)	Decomposition/ reaction temperature (K)	Main events	Species peaks
NC	0.8	430	Decomposition of NC	$\text{NO}^+$ $\text{O}^+$ $\text{CO}_2^+$ $\text{CO}^+/\text{N}_2^+$
$\text{AgIO}_3/\text{CB}$	1.1	570	Reaction between $\text{AgIO}_3$ and CB	$\text{CO}_2^+$
	1.5	740	Decomposition of $\text{AgIO}_3$	$\text{O}^+$ $\text{O}_2^+$ $\text{Ag}^+$ $\text{I}^+$
$\text{AgIO}_3/\text{CB}/\text{NC}$	0.8	360	Decomposition of NC	$\text{NO}^+$ $\text{O}^+$ $\text{CO}_2^+$ $\text{CO}^+/\text{N}_2^+$
	1.5	670	Reaction between $\text{AgIO}_3$ and CB	$\text{CO}_2^+$
	1.6	710	Decomposition of $\text{AgIO}_3$	$\text{I}^+$ $\text{Ag}^+$ $\text{O}^+$ $\text{O}_2^+$

Heating rate is  $\sim 6 \times 10^5 \text{ K}^{-1}$

release. The possible formation pathway of the rain or snow using  $\text{AgIO}_3/\text{CB}/\text{NC}$  composite is shown in Fig. 7. After the ignition, the primary flame propagated from one side to the other with gaseous products and heat was released to activate the secondary flame. AgI nanoparticles as nucleus for ice formation due to lattice constant  $4.5922 \times 7.51$ , being close to that of ice ( $4.535 \times 7.41$ ).

## Conclusions

Silver iodide (AgI) nanoparticles with a mean diameter from 51 to 97 nm were produced by an on-the-fly combustion/generation of  $\text{AgIO}_3/\text{CB}/\text{NC}$  composites produced by electro spray deposition. The resultant particles are considered as candidate for a cloud-seeding pyrotechnic, without toxic residual by-

products. For  $\text{AgIO}_3/\text{CB}/\text{NC}$  film, the flame propagation velocity in air increases with the increasing particle mass loading of  $\text{AgIO}_3$  and CB, and peaks at about 40 wt% ( $\text{AgIO}_3/\text{CB}$  over NC). At 60 wt%, no self-propagation in the film of  $\text{AgIO}_3/\text{CB}/\text{NC}$  is obvious. The mass loading of  $\text{AgIO}_3$  and CB played a major role in size control of the AgI nanoparticles. In the  $\text{AgIO}_3/\text{CB}/\text{NC}$  films, the mean diameter of the obtained AgI particles gradually increased to a larger size from 51 to 97 nm with the mass loading of  $\text{AgIO}_3/\text{CB}$  increased from 10 to 50 wt%. The combustion flame of  $\text{AgIO}_3/\text{CB}/\text{NC}$  composite is composed of primary flame and secondary flame, and the primary flame front is consistent with the decomposition of NC and its reaction with  $\text{O}_2$ . The secondary flame front is caused by the reaction between  $\text{AgIO}_3$  and CB, and the decomposition of  $\text{AgIO}_3$  with AgI nanoparticle release. Compared with the reference AgI/AP/NC

and AgIO<sub>3</sub>/Al/NC films, AgIO<sub>3</sub>/CB/NC performed the best for the application of weather modification.

**Acknowledgments** This work was carried out with the support of the Defence Threat Reduction Agency. Xiuli Hu is grateful for the financial support from China Scholarship Council.

## References

- Biswas KR, Dennis AS (1971) Formation of a rain shower by salt seeding. *J Appl Meteorol* 10:780–784
- Blair D, Davis B, Dennis A (1973) Cloud chamber tests of generators using acetone solutions of AgI-NaI, AgI-KI and AgI-NH<sub>4</sub>I. *J Appl Meteorol* 12:1012–1017
- Burley G (1963) Structure of hexagonal silver iodide. *J Chem Phys* 38:2807–2812. doi:10.1063/1.1733606
- Changnon SA (1977) The scales of hail. *J Appl Meteorol* 16:626–648
- DeMott PJ (1988) Comparisons of the behavior of AgI-type ice nucleating aerosols in laboratory- simulated clouds. *J Chem Inf Model* 20:44–50. doi:10.1017/CBO9781107415324.004
- Dennis AS (1980) Weather modification by cloud seeding. International Geophysics series, vol 24. Academic Press, New York, pp 96–133
- Egan GC, Sullivan KT, Lagrange T et al (2014) In situ imaging of ultra-fast loss of nanostructure in nanoparticle aggregates. *J Appl Phys* 115:084903. doi:10.1063/1.4867116
- Federer B, Schneider A (1981) Properties of pyrotechnic nucleants used in grossversuch IV. *J Appl Meteorol* 20:997–1005
- Guo X, Zheng G, Jin D (2006) A numerical comparison study of cloud seeding by silver iodide and liquid carbon dioxide. *Atmos Res* 79:183–226. doi:10.1016/j.atmosres.2005.04.005
- He Y, Wu F, Sun X et al (2013) Factors that affect pickering emulsions stabilized by graphene oxide. *ACS Appl Mater Interfaces* 5:4843–4855. doi:10.1021/am400582n
- Hu X, DeLisio J, Li X, et al (2016) Direct deposit of highly reactive Bi(IO<sub>3</sub>)<sub>3</sub>- polyvinylidene fluoride biocidal energetic composite. *Adv Eng Mater* (In press)
- Huang C, Jian G, DeLisio JB et al (2015) Electrospray deposition of energetic polymer nanocomposites with high mass particle loadings: a prelude to 3D printing of rocket motors. *Adv Eng Mater* 17:95–101. doi:10.1002/adem.201400151
- Jian G, Chowdhury S, Sullivan K, Zachariah MR (2013) Nanothermite reactions: is gas phase oxygen generation from the oxygen carrier an essential prerequisite to ignition? *Combust Flame* 160:432–437. doi:10.1016/j.combustflame.2012.09.009
- Li X, Guerieri P, Zhou W et al (2015) Direct deposit laminate nanocomposites with enhanced propellant properties. *ACS Appl Mater Interfaces* 7:9103–9109. doi:10.1021/acsami.5b00891
- Liu W, Zhou J, Jin W et al (2011) A kind of late-model solid AgI composition which is vacuum casting and high temperature. *Jianxi Sci* 29:29–33 (In Chinese)
- Mather GK, Terblanche DE, Steffens FE, Fletcher L (1997) Results of the South African cloud-seeding experiments using hygroscopic flares. *J Appl Meteorol* 36:1433–1447. doi:10.1175/1520-0450(1997)036<1433:ROTSAC>2.0.CO;2
- Meeks K, Pantoya ML, Apblett C (2014) Deposition and characterization of energetic thin films. *Combust Flame* 161:1117–1124. doi:10.1016/j.combustflame.2013.10.027
- Orville HD (1996) A review of cloud modeling in weather modification. *Bull Am Meteorol Soc* 77:1535–1555
- Orville HD, Farley RD, Hirsch JH (1984) Some surprising results from simulated seeding of stratiform-type clouds. *J Clim Appl Meteorol* 23:1585–1600
- Pearce JN, Wirth VI (1933) The potential of the silver-silver iodate electrode at 25°. *J Am Chem Soc* 55(9):3569–3571
- Ryan BF, King WD (1997) A critical review of the Australian experience in cloud seeding. *Bull Am Meteorol Soc* 78:239–254. doi:10.1175/1520-0477(1997)078<0239:ACROTA>2.0.CO;2
- Sax RI, Garvey DM, Parungo FP (1979) Characteristics of AgI pyrotechnic nucleant used in NOAA's Florida area cumulus experiment. *J Appl Meteorol* 18:195–202
- Schaefer VJ (1946) The production of ice crystals in a cloud of supercooled water droplets. *Science* 104:457–459
- Su Z (2008) A laboratory study on nucleating properties of silver iodide-type pyrotechnics. Nanjing University of Information Science and Technology (In Chinese)
- Sullivan KT, Piekielek NW, Chowdhury S et al (2011) Ignition and combustion characteristics of nanoscale Al/AgIO<sub>3</sub>: a potential energetic biocidal system. *Combust Sci Technol* 183:285–302. doi:10.1080/00102202.2010.496378
- Sullivan KT, Piekielek NW, Wu C et al (2012) Reactive sintering: an important component in the combustion of nanocomposite thermites. *Combust Flame* 159:2–15. doi:10.1016/j.combustflame.2011.07.015
- Turns SR (2000) An introduction to combustion: concepts and applications, 2nd edn. McGraw-Hill Companies Inc, Boston, pp 1–620
- Vonnegut B (1947) The nucleation of ice formation by silver iodide. *J Appl Phys* 18:593–595. doi:10.1063/1.1697813
- Weather Modification Association WMA (2009) Position statement on the environmental impact of using silver iodide as a cloud seeding agent. [http://www.weathermodification.org/images/AGI\\_toxicity.pdf](http://www.weathermodification.org/images/AGI_toxicity.pdf). Accessed July 2009
- Wei Z, Jiangning W, Xiaoning R et al (2007) An investigation on thermal decomposition of DNTF-CMDB propellants. *Propellants Explos Pyrotech* 32:520–524. doi:10.1002/prop.200700052
- Westrum F, Arbor A (1989) Heat capacity, thermodynamic properties, and transitions of silver iodide. *J Chem Thermodyn* 21:631–651
- Yao X, Liu T, Liu X et al (2014) Loading of CdS nanoparticles on the (101) surface of elongated TiO<sub>2</sub> nanocrystals for efficient visible-light photocatalytic hydrogen evolution from water splitting. *Chem Eng J* 255:28–39. doi:10.1016/j.cej.2014.06.055
- Zenin A (1995) HMX and RDX—Combustion mechanism and influence on modern double-base propellant combustion. *J Propuls Power* 11:752–758. doi:10.2514/3.23900

Zhou L, Piekiet N, Chowdhury S, Zachariah MR (2009) T-jump/time-of-flight mass spectrometry for time-resolved analysis of energetic materials. *Rapid Commun Mass Spectrom* 23:194–202

Zhou L, Piekiet N, Chowdhury S, Zachariah MR (2010) Time-resolved mass spectrometry of the exothermic reaction between nanoaluminum and metal oxides : the role of oxygen release. *J Phys Chem C* 114:14269–14275